



HHS Public Access

Author manuscript

Nat Commun. Author manuscript; available in PMC 2012 December 24.

Published in final edited form as:

Nat Commun. ; 3: 902. doi:10.1038/ncomms1905.

Impaired Thermogenesis and Adipose Tissue Development in Mice with Fat-Specific Disruption of Insulin and IGF-1 Signalling

Jeremie Boucher¹, Marcelo A. Mori^{1,3}, Kevin Y. Lee¹, Graham Smyth¹, Chong Wee Liew¹, Yazmin Macotella^{1,4}, Michael Rourk¹, Matthias Bluher², Steven J. Russell¹, and C. Ronald Kahn¹

¹Section on Integrative Physiology and Metabolism, Joslin Diabetes Center and Department of Medicine, Brigham and Women's Hospital and Harvard Medical School, Boston, MA, 02215, USA

²Department of Medicine, University of Leipzig, 04103 Leipzig, Germany

Abstract

Insulin and insulin-like growth factor 1 (IGF-1) play important roles in adipocyte differentiation, glucose tolerance and insulin sensitivity. Here, to assess how these pathways can compensate for each other, we created mice with a double tissue-specific knockout of insulin and IGF-1 receptors to eliminate all insulin/IGF-1 signaling in fat. These FIGIRKO mice had markedly decreased white and brown fat mass and were completely resistant to high fat diet (HFD) induced obesity and age- and HFD-induced glucose intolerance. Energy expenditure was increased in FIGIRKO mice despite a >85% reduction in brown fat mass. However, FIGIRKO mice were unable to maintain body temperature when placed at 4°C. Brown fat activity was markedly decreased in FIGIRKO mice but was responsive to β 3-receptor stimulation. Thus, insulin/IGF-1 signaling has a crucial role in the control of brown and white fat development, and, when disrupted, leads to defective thermogenesis and a paradoxical increase in basal metabolic rate.

Keywords

Insulin and IGF-1 receptors; Obesity; Brown and White adipose tissue; Adipocyte differentiation; Thermogenesis; Glucose tolerance

Users may view, print, copy, download and text and data- mine the content in such documents, for the purposes of academic research, subject always to the full Conditions of use: http://www.nature.com/authors/editorial_policies/license.html#terms

Corresponding author: C. Ronald Kahn, MD, Joslin Diabetes Center, One Joslin Place, Boston, MA 02215, Phone: (617)732-2635, Fax: (617)732-2487, c.ronald.kahn@joslin.harvard.edu.

³Current address: Department of Biophysics, Federal University of São Paulo. São Paulo, Brazil

⁴Current address: Instituto de Neurobiología, Universidad Nacional Autónoma de México. Queretaro, México. 76230

AUTHOR CONTRIBUTIONS

JB designed and performed experiments, analyzed data and wrote the paper; MAM designed and performed experiments; GS and MB performed experiments and analyzed data; KYL, CWL, YM, MR and SJR performed experiments; CRK designed experiments, analyzed data and helped write the paper.

COMPETING FINANCIAL INTERESTS STATEMENT

The research in this paper was supported entirely by NIH funding; however, Dr. Kahn is a founder and member of the Scientific Advisory Board of Ember Therapeutics, which is interested in adipose tissue as a target for therapy of diabetes and obesity

INTRODUCTION

Obesity, i.e., excess body fat, is associated with the development of metabolic disorders such as type 2 diabetes, hyperlipidemia and cardiovascular disease and fatty liver¹. Obesity results from an imbalance between energy expenditure and energy intake resulting in a positive energy balance. White adipose tissue is the main energy storage organ in the body, whereas brown adipose tissue (BAT) is an essential component of energy expenditure by dissipating energy as heat through uncoupled respiration mediated by uncoupling protein 1 (UCP1). While BAT persists after birth in small mammals, its presence in humans was thought to be limited to newborns. However, recent studies using positron emission tomography (PET) imaging have shown that BAT is present in adult humans and is functionally active²⁻⁶.

Both white and brown adipose tissue development and expansion occur through differentiation of preadipocytes into adipocytes, as well as storage and mobilization of lipids. Many paracrine and endocrine factors control adipose tissue development⁷. Among them, insulin and IGF-1 play an essential role in stimulating cell proliferation, differentiation and lipid accumulation^{8,9}. Both insulin receptors (IR) and IGF-1 receptors (IGF1R) are present in preadipocytes and adipocytes, with more IGF1R in preadipocytes and more IR in adipocytes¹⁰⁻¹².

While insulin and IGF-1 bind preferentially to their cognate receptors, we have shown that IR and IGF1R can act as identical portals in the regulation of gene expression and adipocyte differentiation in preadipocytes¹². Thus, when the IR^{13,14} or IGF1R¹⁵ is inactivated in adipose tissue, the other member of this receptor family can take over part or all of its functions.

In the present study we have investigated the role of insulin and IGF-1 signaling in adipose tissue by creating mice lacking the IR and IGF1R in both white and brown adipose tissues by gene targeting using a Cre recombinase driven by the adipose-specific aP2 promoter. We show that Fat specific IGF1R and IR KO (FIGIRKO) mice are resistant to age-associated and diet-induced obesity and the associated glucose intolerance. Even more striking is the almost complete absence of brown adipose tissue and dramatic cold sensitivity in these mice. Nonetheless, these mice exhibit increased basal energy expenditure. Thus, insulin and IGF-1 signaling play a crucial role in controlling white and brown fat development, adipocyte metabolism and thermogenesis.

RESULTS

FIGIRKO mice show reduced white and brown adipose tissues

To investigate the overlapping signaling created by insulin and IGF-1, we created mice with a combined tissue specific knockout of the insulin and IGF-1 receptors (IR/IGF1R) in fat by breeding mice with IR and IGF1R floxed alleles with mice carrying an aP2 promoter-Cre transgene. On normal chow, body weight of male FIGIRKO mice was decreased by 16% at 4 weeks, and this increased to a 42% reduction by 1 year of age (Figure 1a). Epididymal and inguinal fat pad weights at 4 months were decreased by 24% and 53%, respectively (Figure

1b). Even more striking was the >85% reduction in brown adipose tissue (BAT) (Figure 1b). Weights of other tissues were unchanged (Supplementary Figure S1a). There was no difference in cell size in the perigonadal or subcutaneous WAT between FIGIRKO and control mice, indicating that the decrease in fat mass was due to fewer, not smaller, white adipocytes (Figure 1c and d). On the other hand, there was a reduction in lipid content in BAT from FIGIRKO mice (Figure 1c) and a 17.2% decrease in cell diameter, indicating a decrease in both cell number and cell size in this depot. Lean mass was decreased by 10% in FIGIRKO mice, but slightly increased when normalized to total body weight, indicating that the decrease in body weight observed in FIGIRKO mice was mostly attributed to a decrease in fat mass (Supplementary Figure S1b). Skeletal muscle weights were not different between control and FIGIRKO mice (Supplementary Figure S1c), but femur length was decreased in FIGIRKO mice by 2–6% suggesting a mild growth defect (Supplementary Figure S1d). White adipose tissue at 6 weeks old was reduced by \approx 20% in FIGIRKO mice, whereas interscapular BAT was decreased by 84% (Supplementary Figure S2a,b). IR and IGF1R mRNA levels in the remaining WAT and BAT and isolated WAT adipocytes of FIGIRKO mice were decreased 30–60% compared to control, with no change in other tissues (Supplementary Figure S3).

FIGIRKO mice are protected against glucose intolerance

In 4 month old mice, fed and fasted glucose and insulin levels (Supplementary Figure S4a,b), and glucose tolerance (Supplementary Figure S4c) were all similar between control and FIGIRKO mice. However, by 1 year of age fasting glucose (Figure 2a) and glucose tolerance was better in FIGIRKO mice than controls (Figure 2b). This occurred without any difference in insulin sensitivity as measured by ITT (Figure 2c) or glucose-stimulated insulin secretion (Figure 2d). However, the glucose infusion rate required to maintain euglycemia during a hyperinsulinemic-euglycemic clamp was 25% higher in FIGIRKO than in controls, indicating an increase in insulin sensitivity (Figure 2e). Insulin stimulated whole-body glucose disposal was also increased by 51% in FIGIRKO mice; this was paralleled by an increase in basal endogenous glucose production (Figure 2e). Insulin-stimulated glucose uptake assessed during the clamp using ^{14}C -2-deoxyglucose was decreased by 50% in white adipose tissue from FIGIRKO mice, but increased by 1.6–2.3-fold in skeletal muscle (Figure 2f) indicating that the better glucose tolerance of FIGIRKO mice is due to increased glucose uptake in muscle.

FIGIRKO mice are protected against HFD-induced obesity

When challenged with a HFD for 4 months control mice rapidly developed obesity with a 75% increase in body weight, while FIGIRKO mice were completely protected from HFD-induced weight gain (Figure 3a). Accordingly, perigonadal and inguinal adipose tissue in FIGIRKO mice were markedly reduced to 28% and 8% of those in control mice after the HFD (Figure 3b). Adipocyte cell size was again not different between control and FIGIRKO mice indicating that FIGIRKO mice are protected from obesity by having reduced adipocyte number. BAT mass in HFD fed FIGIRKO mice was also reduced by 83% when compared to controls and showed reduced lipid content (Figure 3b).

Adipocyte lipid content reflects a balance between synthesis, which is dependent on glucose uptake by glucose transporter 4 (GLUT4) and fatty acid synthase (FAS), and triglyceride breakdown, dependent on hormone sensitive lipase (HSL) and adipocyte triglyceride lipase (ATGL). In perigonadal fat, there was no difference in FAS, GLUT4, HSL or ATGL expression between control and FIGIRKO mice fed either a chow or HFD (Figure 3c). There was also no difference in expression of these genes in subcutaneous adipose tissue fed a chow diet. However, there were 58–76% reductions of FAS, GLUT4, HSL and ATGL in subcutaneous fat from HFD fed FIGIRKO mice compared to control. FAS, GLUT4, HSL and ATGL were also decreased by 42–85% in BAT from FIGIRKO mice on either chow or high fat diet (Figure 3c).

Consistent with the difference in weight gain, glucose tolerance worsened in control mice on HFD, but remained unchanged in FIGIRKO mice (Figure 4a). This occurred without improvement in insulin sensitivity as measured by ITT (Figure 4b) or difference in glucose-stimulated insulin secretion (Figure 4c). Random fed insulin levels, however, were elevated 6-fold in FIGIRKO mice after HFD compared to controls, possibly contributing to the improved glucose tolerance (Table 1). Circulating levels of adiponectin, leptin and resistin were decreased by 42, 60 and 65% in FIGIRKO mice compared to control mice (Table 1), consistent with the reduced expression of these genes in perigonadal and subcutaneous adipose (Supplementary Figure S5a).

Obesity is often associated with hepatic steatosis. Analysis of livers from control mice on HFD revealed a 3.5-fold increase in lipid content compared to mice fed regular chow (1.03 ± 0.17 vs. 3.61 ± 0.99 mg triglyceride/100 mg liver). Livers from FIGIRKO mice on HFD were 20% heavier and accumulated 1.9 times more lipid than control mice (Figure 4d and e). Serum triglyceride and free fatty acid levels also trended to be elevated in FIGIRKO mice on HFD, whereas cholesterol levels and circulating levels of TNF α , IL6 and PAI-1 were similar (Table 1). As expected, HFD resulted in increases in inflammatory markers (TNF α , MCP1 and F4/80) in both perigonadal and subcutaneous WAT of control mice. Interestingly, there was a similar increase in expression of these genes in FIGIRKO adipose tissue (Supplementary Figure S5b). Thus, FIGIRKO mice on HFD develop inflammatory changes in adipose tissue to those of control despite the much smaller fat pad size.

Increased energy expenditure in FIGIRKO mice

Alterations in body weight are the balance between energy intake and energy expenditure. Food intake was similar between control and FIGIRKO mice fed either chow or HFD, suggesting that the reduction in adipose mass was due to increased energy expenditure (Figure 5a). Indeed, oxygen consumption rates assessed by indirect calorimetry revealed a 15% increase in VO₂ per gram of lean body weight in FIGIRKO mice on a chow diet (Supplementary Figure S4d). This occurred with no change in spontaneous activity (Figure 5b). Indirect calorimetry performed in a separate cohort of FIGIRKO mice fed a HFD from 6 to 10 months of age confirmed a complete resistance to diet-induced obesity (Figure 5c and Supplementary Figure S6a,b). Energy expenditure was again increased in FIGIRKO mice compared to control mice by 13–14% during the dark cycle and 7–8% during the light cycle on standard chow and high fat diet (Figure 5d), with no difference in RER between

control and FIGIRKO mice (Figure 5e). Together, these results indicate that the decreased fat mass observed in FIGIRKO mice was due to a combination of a decrease in the number of adipocytes and an increase in energy expenditure.

Decreased adipocyte differentiation in FIGIRKO mice and cells

Adipocyte differentiation depends on the regulation of a transcriptional regulatory cascade involving PPAR γ and proteins from the C/EBP family. In perigonadal fat, expression of C/EBP α and C/EBP β , as well as the adipocyte marker aP2, was unchanged in FIGIRKO mice compared to controls on both chow and HFD, whereas PPAR γ expression was reduced by \approx 40% in fat of HFD fed FIGIRKO mice. In subcutaneous fat, PPAR γ , C/EBP α , C/EBP β and aP2 were all decreased 20 to 70% in FIGIRKO mice fed either chow or HFD (Supplementary Figure S5c). For BAT, the decrease in these adipocyte differentiation genes was even more pronounced, with all four genes down-regulated 20 to 90% in chow diet or HFD fed FIGIRKO mice (Figure 6a).

To better understand the reduction in adipose tissue mass and expression of key differentiation factors in FIGIRKO fat, we investigated the effect of knockout of the IR and IGF1R genes in brown preadipocytes in vitro¹⁶. Eight days after induction of differentiation, wild-type (WT) cells accumulated abundant lipid droplets which stained with Oil Red O (Figure 6b). By contrast, no lipid accumulation was apparent in the IR and IGF1R double knockout (DKO) cells, indicating that insulin/IGF-1 signaling is critical for adipocyte differentiation. Addition of either the PPAR γ agonist rosiglitazone or the brown adipogenesis inducer BMP-7 (ref. 17) were unable to rescue the lack of differentiation observed in DKO cells. This difference in adipocyte differentiation was also apparent in measurement of expression of adipocyte markers, which increased progressively at the mRNA and protein level in WT cells, but failed to be induced in DKO cells (Figure 6c,d).

As expected, PPAR γ and C/EBP α mRNAs both increased by $>$ 20-fold in WT cells during adipocyte differentiation. By contrast, PPAR γ and C/EBP α did not increase in DKO cells, indicating that insulin/IGF-1 signaling acts upstream of C/EBP α and PPAR γ to induce adipocyte differentiation (Figure 6d), most likely on C/EBP β and C/EBP δ ^{18, 19}. C/EBP β and C/EBP δ mRNA increased 20-fold rapidly after induction of differentiation both in WT and DKO cells (Supplementary Figure S7). This was confirmed at the protein level (Figure 6e). However, C/EBP β phosphorylation at threonine 188, which leads to DNA binding and transactivation of C/EBP α and PPAR γ genes^{20, 21}, was significantly reduced in DKO cells, both under basal conditions and after addition of the induction cocktail (Figure 6f). However, cellular localization of C/EBP β and δ was normal in DKO cells compared to WT cells. Thus, insulin and IGF-1 signaling play a critical role in adipocyte differentiation, controlling C/EBP β phosphorylation and activation upstream of C/EBP α and PPAR γ .

Impaired thermogenesis in FIGIRKO mice

Although brown adipose tissue is involved in thermogenesis, basal body temperature was similar between control and FIGIRKO mice (Supplementary Figure S8a) raised at \approx 21°C. However, when put in a 4°C environment, FIGIRKO mice were unable to maintain their body temperature. Thus, while control mice dropped their body temperature by only 3.5°C

after 90 min under these conditions, FIGIRKO mice dropped their body temperature by 12.6°C, and all FIGIRKO mice had to be removed from the cold before 2 hours due to a drop of their body temperature below 25°C (Figure 7a). By contrast, mice with a fat specific insulin receptor KO (FIRKO mice) that have a 50% reduction in BAT mass¹⁴ and mice with a fat specific knockout of the IGF1R that have normal BAT mass showed normal thermoregulation at 4°C (Supplementary Figure S8b,c). This defect was due to the major reduction in BAT mass in FIGIRKO mice, as well as a decrease in expression of genes involved in thermogenesis and various BAT markers. Thus, BAT from FIGIRKO mice had a 40% decrease in UCP1 mRNA levels compared to control (Figure 7b), and this was paralleled by 41–75% decreases in PGC1 α , PRDM16, Tfam, Nrf1, UCP3 and beta-adrenergic receptors Adrb1, 2 and 3 (Figure 7c and Supplementary Figure S8d). Interestingly, expression of other BAT markers, such as Dio2, Elovl3 and Cox2 was not changed in BAT from FIGIRKO mice compared to control (Supplementary Figure S8d), indicating that BAT from FIGIRKO mice has some alterations in differentiated function, but not a complete failure of differentiation.

To determine BAT activity and its activation by β -adrenergic stimulation *in vivo*, we performed ¹⁸F-fluorodeoxyglucose (FDG) positron-emission tomographic and computed tomographic (PET–CT) scans in control and FIGIRKO mice before and after intraperitoneal injection of the selective β 3 adrenergic receptor agonist CL316243. Under basal conditions, FDG uptake was five times higher in BAT from control mice compared to FIGIRKO mice (Figure 7d). One hour after CL316243 injection, FDG uptake increased 1.9-fold in BAT of control mice, and 5.2-fold in BAT from FIGIRKO mice, but uptake in FIGIRKO mice was still reduced by 45% compared to stimulated controls. When adjusted for the size differences in interscapular brown fat between the control and knockout mice, total FDG uptake was 35 and 13 times higher in BAT from control mice compared to FIGIRKO mice under basal and CL316243-activated conditions, respectively (Figure 7d). Thus BAT from FIGIRKO mice is dramatically reduced compared to BAT from control mice, but is still responsive to β 3 adrenergic stimulation.

We also measured gene expression in white and brown adipose tissues of mice injected with CL316243. After 3 hours, UCP1 mRNA levels increased 45-fold and 4-fold in PG and SC white adipose tissues of control mice, but not in BAT, probably due to the already extremely high UCP1 expression level in this tissue (Figure 7e). In FIGIRKO mice, CL316243 induced an even greater increase in UCP1 with 175-fold and 20-fold increases in PG and SC, respectively. Similarly, CL316243 induced an increase in PGC1 α and Elovl3 mRNA levels in adipose tissues of both control and FIGIRKO mice. These results indicate that absence of insulin and IGF-1 signaling in fat does not prevent the increased expression of genes involved in cold induced thermogenesis. Thus, the cold sensitivity observed in FIGIRKO mice is likely due to the dramatic reduction in BAT mass and alteration in expression of key thermogenic genes, rather than an absence of induction of cold-induced stimulated genes. However, other potential mechanisms for the cold sensitivity such as decreased free fatty acid supply, decreased skeletal muscle ability to shiver or impaired heart or lung function cannot be excluded.

Systemic brown adipocytes differ from the discrete or preformed interscapular brown adipose tissue depot in their developmental origin^{22, 23}. They are found mixed in white fat and between muscle bundles²⁴, arise from different progenitors than the cells giving rise to the preformed BAT, and are inducible by β 3-adrenergic receptor stimulation and cold exposure. Daily injections of CL316243 for 2 weeks led to formation of systemic brown adipocytes within PG and SC white adipose tissue in control mice, as indicated by the increase in brown fat markers, histology and UCP1-immunostaining of fat from treated mice (Supplementary Figure S9a,b). Interestingly, FIGIRKO mice also accumulated newly formed brown adipocytes in PG and SC adipose tissue depots to a similar extent than in control mice, indicating that while insulin/IGF-1 signaling is essential for preformed brown adipose tissue formation, this pathway appears to be less important in the differentiation of systemic brown fat.

DISCUSSION

Insulin and IGF-1 act through highly homologous receptors to initiate their functions on metabolism and growth. While insulin and IGF-1 can have distinct physiological roles, at the cellular level they regulate many of the same signaling pathways. We have previously shown that the IR and IGFR have similar effects in regulating gene expression in preadipocytes, with the main difference between insulin and IGF-1 effects being due to a modulation in amplitude of the signal created by the specific ligand-receptor interaction¹². To understand the role of complementary actions of insulin and IGF-1 in fat metabolism and development, we created mice with a combined knockout of IR and IGFR in fat using Cre recombinase under the control of the adipocyte specific aP2 promoter. The resulting FIGIRKO mice exhibit reduced body weight, reduced white adipocyte number and an almost complete absence of brown adipose tissue with dramatic sensitivity to cold exposure. Nonetheless, these mice are completely protected from age- and HFD-induced obesity and glucose intolerance, at least in part, due to increased energy expenditure and increased glucose uptake in skeletal muscle.

From the data, it appears that these changes occurred with only a partial knockdown of IR and IGFR, since the mRNA levels of these two receptors in different fat depots were reduced only 30 to 60% in FIGIRKO mice. However, this is almost certainly an underestimate of the efficiency of the knockout, since inactivation of both IR and IGFR dramatically impairs adipocyte differentiation, and in vivo, we can only assess the degree of inactivation in the residual adipose tissue in which the cells may have recombined some, but not all four, targeted alleles. This marked impairment of adipose tissue development, with some escaping cells, is consistent with the reduced number of normal sized adipocytes observed in adipose tissues from FIGIRKO mice and is more than sufficient to produce a strong whole body phenotype.

The phenotype of the FIGIRKO mice differs drastically from that of mice with a fat specific knockout of the insulin receptor (FIRKO). While both mice have reduced white fat mass, this change is much greater in FIGIRKO mice where there is a decrease in cell number compared to FIRKO mice where there is primarily a change in cell size. Both FIRKO and FIGIRKO mice are protected against age-associated glucose intolerance and diet-induced

obesity and glucose intolerance, and both display increased energy expenditure^{14, 25}. On the other hand, FIGIRKO mice are extremely cold sensitive and unable to exhibit an adequate thermogenic response when placed in the cold, whereas FIRKO mice show normal temperature regulation, indicating that the combined inactivation of the IR and IGF1R mediates some additional effects from that of IR alone on BAT development and function.

These additional effects of the IGF1R are only observed when combined with a deletion of the IR. Thus, mice with adipocyte specific deletion of IGF1R only have normal BAT mass, normal temperature regulation and even an increase in white adipose tissue mass. The latter is part of a generalized increase in somatic growth, which has been attributed to increased circulating IGF-1 in these mice¹⁵. However, FIGIRKO mice have normal IGF-1 levels. The reduction in both white and brown adipocyte numbers in FIGIRKO mice reflects the important and synergistic roles of insulin and IGF-1 on the control of white and brown adipocyte differentiation.

Both white and brown adipose tissues from FIGIRKO mice show reductions in adipocyte differentiation markers. Furthermore, IR and IGF1R double knockout brown preadipocytes (DKO) fail to accumulate lipids or increase expression of adipocyte markers after induction of differentiation. C/EBP β phosphorylation was strongly reduced in DKO cells, both under basal conditions or after induction of differentiation, indicating that insulin and IGF-1 signaling play a critical role in the control of adipocyte differentiation via activation and phosphorylation of C/EBP β leading to impaired induction of C/EBP α and PPAR γ .

Interestingly, while insulin and IGF-1 signaling are essential for adipose development in the preformed, discrete brown adipose tissue depots, they may not be required for differentiation of systemic brown adipocytes. These differences may be due to the differential lineages of these different brown fat depots^{22, 23}. This is also suggested by different molecular responses of precursors from these depots to a stimulation by a PPAR γ agonist²⁶. It is also possible that this pool of brown preadipocytes has a low level of aP2 expression compared to the preformed depot, limiting the extent of receptor inactivation in this population of cells.

FIGIRKO mice are protected against age- and HFD-induced glucose intolerance. Interestingly, expression of inflammatory markers in adipose tissue and circulating cytokine levels are increased in FIGIRKO mice on high fat diet to a similar level as in control mice, ruling out reduced inflammation in fat as a cause for the improved glucose tolerance observed in these mice. Improved glucose tolerance is also not due to differences in insulin secretion. However, insulin-stimulated glucose uptake is increased in skeletal muscle from FIGIRKO mice, and coupled with the increased insulin levels in HFD-fed FIGIRKO mice, it seems likely that the better glucose tolerance of FIGIRKO mice is due to increased insulin action in skeletal muscle.

The most dramatic finding in FIGIRKO mice is the almost complete absence of interscapular BAT, highlighting the crucial role for insulin/IGF-1 signaling in BAT formation. BAT mass/activity in humans is inversely correlated with body mass index and percent body fat^{2-4, 27-29}. Interestingly, the defect in brown fat development in FIGIRKO

mice is associated with increased energy expenditure and leanness. Although surprising, this is in agreement with the phenotype observed in UCP1 deficient mice which are cold sensitive³⁰ and protected from HFD-induced obesity when raised at 20°C³¹, but can become obese on HFD in a thermoneutral (29°C) environment³². This suggests that for BAT to have a role in regulating energy expenditure, the tissue must have functional insulin and IGF-1 receptors. Exactly how FIGIRKO mice maintain temperature at 21°C is unclear, since FIGIRKO mice do not show increased systemic brown adipocytes or increased expression of any UCP in muscle, fat or liver. Nevertheless, at 4°C FIGIRKO mice are unable to maintain their body temperature, indicating that brown fat is essential for adaptive thermogenesis, similar to what has been observed in mice with UCP1 inactivation³⁰. However, UCP1 deficient mice can be kept at 4°C if they are gradually adapted to the cold^{33,34}, but this is due to shivering rather than the development of BAT-related thermogenesis^{33,35}.

Cold induced thermogenesis is mediated via the sympathetic nervous system through activation of β -adrenergic receptors^{36,37}. Despite the small BAT mass, the increase in FDG uptake after β 3 stimulation is greater in FIGIRKO mice than controls. Furthermore, the β 3 adrenergic agonist induced UCP1, PGC1 α and Elovl3 expression in white and brown adipose tissues from both control and FIGIRKO mice to the same extent. However, the relative amount of FDG uptake is still lower in BAT from FIGIRKO mice in both basal and stimulated conditions indicating that in addition to the reduced BAT mass, BAT from FIGIRKO mice is less active.

Taken together, these results highlight the critical role of insulin and IGF-1 signaling in the control of white and brown adipose tissue development and function, as well as the regulation of glucose metabolism and energy expenditure.

MATERIAL AND METHODS

Animals and diets

Mice were housed in a temperature-controlled (20–22°C) room on a 12 h-light/dark cycle in an animal facility at the Foster Biomedical Research Laboratory of Brandeis University in Waltham, MA. All protocols were approved by the Institutional Animal Care and Use Committee of the Joslin Diabetes Center and Brandeis University and were in accordance with NIH guidelines. Mice were allowed *ad libitum* access to water and food. aP2-Cre from the Barbara Kahn laboratory and double IR and IGF1R floxed animals have been described previously^{38,39}. Control and fat specific IR and IGF1R KO (FIGIRKO) mice were maintained on a mixed (C57Bl/6 – 129Sv) background by breeding aP2-Cre IR^{ff}/IGF1R^{ff} with IR^{ff}/IGF1R^{ff} mice. Animals were maintained on a standard chow diet containing 22% calories from fat, 23% from protein, and 55% from carbohydrates (Mouse Diet 9F 5020; PharmaServ), or subjected to a high fat diet (HFD) containing 60% calories from fat, 20% from protein, and 20% from carbohydrates (OpenSource Diet D12492, Research Diet). Fat specific insulin receptor knockout (FIRKO) mice and fat specific IGF-1 receptor knockout mice (IGF-1RaP2Cre) have been described previously^{14,15}.

Adipocyte cell size

Adipocytes from perigonadal and subcutaneous adipose tissue depots were dissected, minced, and digested with 1 mg/mL collagenase I (Worthington Biosciences) in D-MEM high glucose supplemented with 1% bovine serum albumin (BSA), shaking for 30 minutes at 37°C. Cells were passed through a 200 µM filter and washed twice with D-MEM high glucose plus BSA. Cells were fixed with osmium tetroxide, rinsed twice with PBS, and aliquots were used to take pictures on microscope slides. Adipocyte diameter from cells bigger than 20 µM was determined using Image J software. At least 5 pictures representing a total of ≈ 1000 per adipose tissue depot were used. 4 control and 4 FIGIRKO mice were used, representing a total of ≈ 5000 adipocytes per group. For brown adipocyte cell size, the number of cells/nuclei was determined from hematoxylin and eosin stained sections of brown adipose tissue from 4 FIGIRKO and 4 control mice. Average diameter of cells was determined for each slide.

Metabolic studies

Glucose tolerance and glucose stimulated insulin secretion tests (2 g dextrose/kg body weight injected intraperitoneally) were performed in unrestrained conscious mice after a 16h overnight fast. Insulin tolerance tests (1.25 units insulin/kg body weight injected intraperitoneally, Humulin R, Lilly) were performed after a 2h fast. Glucose levels were measured in blood collected from the tail at the indicated times after injection, with Infinity glucose monitors and strips (US Diagnostics). Insulin sensitivity was directly and more precisely assessed by performing hyperinsulinemic-euglycemic clamps in conscious mice as described previously⁴⁰, with a continuous insulin infusion dose of 2.5 mU/kg/min.

Tissue triglyceride analysis

Lipids from liver samples were extracted with Folch solution consisting of a mixture of 2:1 (v/v) chloroform/methanol. Lipids were solubilized in 1% Triton X-100 and dried by evaporation. Triglyceride content was determined using Triglyceride Determination Kit (Sigma).

Energy expenditure and body composition

For the energy expenditure studies, 12 control and 12 FIGIRKO male mice were shipped to the Vanderbilt Mouse Metabolic Phenotyping Center. Oxygen consumption (VO_2), carbon dioxide (VCO_2) and heat production were measured by indirect calorimetry using the Comprehensive Laboratory Animal Monitoring System (CLAMS; Columbus Instruments) in 6 months old animals fed a chow diet. The respiratory exchange ratio (VCO_2/VO_2) was calculated from the gas exchange data and all data were normalized to lean body mass. Half of the animals were then placed on a high fat diet for 4 months while the others remained on a chow diet and body composition was assessed weekly by nuclear magnetic resonance. VO_2 , VCO_2 and heat production were measured again at the end of the diet.

Body temperature and cold exposure

Body temperatures were assessed in 4 months old mice using a RET-3 rectal probe for mice (Physitemp). For the cold exposure experiment, mice were housed individually and

transferred to a cold room with an ambient temperature of 4°C. Temperature was measured every 30 min for 3 hours or until mouse core body temperature dropped below 25°C.

In vivo BAT Imaging by PET/CT

Mice were anesthetized by intraperitoneal injection of pentobarbital at 75mg/kg. Ten minutes post injection of anesthetic, saline or CL316243 was injected IP at 1mg/kg. Five minutes post injection of drug, mice were then injected retroorbitally with F18-FDG at 200–300µCi. Time and exact amount of injected isotope was noted immediately after injection. Two hours post-injection of ¹⁸F-FDG, mice were imaged by PET/CT on a NanoPET/CT™ (Bioscan) dual modality small animal imager. Thirty minutes prior to PET acquisition, all mice were given a subsequent dose of pentobarbital at 75 mg/kg to ensure adequate anesthetization throughout the duration of the PET/CT scan.

Gene expression analysis

Total RNA was extracted from tissues with Trizol. RNA (1 µg) was reverse-transcribed with a high-capacity complementary DNA (cDNA) reverse transcription kit (Applied Biosystems) according to the manufacturer's instructions. Real-time PCR was performed starting with 12.5 ng of cDNA and both sense and antisense oligonucleotides (300 nM each) in a final volume of 10 µl with the SYBR Green PCR Master Mix (Applied Biosystems). Fluorescence was monitored and analyzed in an ABI Prism 7900 HT sequence detection system (Applied Biosystems). Analysis of TATA box-binding protein (TBP) expression was performed in parallel to normalize gene expression. Amplification of specific transcripts was confirmed by analyzing melting curve profiles at the end of each PCR. Real time PCR primers sequences are listed in Supplementary Table S1.

Cell culture and adipocyte differentiation

DKO brown preadipocyte cell lines were generated from immortalized IR and IGF1R floxed brown preadipocytes infected with an adenovirus encoding *Cre* recombinase as described previously¹⁶. Cells were maintained in Dulbecco's modified Eagle's medium (high glucose) containing 10% (v/v) fetal calf serum at 37 °C in a 5% CO₂ environment. Adipocyte differentiation was induced in confluent WT or DKO preadipocytes by treating confluent cells (day 0) with an induction mixture containing 20 nM insulin and 1 nM triiodothyronine, 0.5 mM isobutylmethylxanthine, 1 µM dexamethasone, and 0.125 mM indomethacin for 48 h. After this induction phase (day 2), cells were kept in medium containing insulin and triiodothyronine for the subsequent 6 days, changing the medium every 2 days. Lipid accumulation was visualized at day 8 by oil red O staining. Cells were washed once with phosphate-buffered saline and fixed with 10% buffered formalin for 1 h. Cells were then stained with filtered oil red O solution (5 g/liter in isopropyl alcohol) diluted 2-fold in water for 1 h at room temperature.

Western blot analysis

Cells were washed once with cold phosphate-buffered saline (PBS) and scraped in radioimmunoprecipitation assay lysis buffer containing 1% SDS, 10 mM glycerophosphate, 10 mM NaF, 0.1 mM sodium orthovanadate, and 1% protease inhibitor cocktail (Sigma).

For cytoplasmic and nuclear extracts, NE-PER Nuclear and Cytoplasmic Extraction Reagents (Thermo Scientific) were used according to manufacturer's instructions. Protein concentrations were determined with the Bradford protein assay (Bio-Rad). Lysates (20 to 40 µg) were subjected to SDS-polyacrylamide gel electrophoresis (SDSPAGE). Proteins were transferred to a polyvinylidene difluoride membrane (Amersham Biosciences) and immunoblotted with the appropriate antibodies. Secondary antibodies were horseradish peroxidase (HRP)-conjugated anti-rabbit immunoglobulin G (IgG) from donkey and HRP-conjugated anti-mouse IgG from sheep (Amersham). Proteins on the membranes were visualized with SuperSignal West Pico substrate or SuperSignal West Dura extended duration substrate (Pierce Biotechnologies). Antibodies (with catalog number) to C/EBPα (sc-61), C/EBPβ (sc-150), C/EBPδ (sc-151), GLUT4 (sc-7938) and UCP1 (sc-6528) were purchased from Santa Cruz Biotechnologies (dilution 1/200). Antibodies to Phospho-C/EBPβ (Thr188) (#3084) and Lamin A/C (#2032) were purchased from Cell Signaling (dilution 1/1000). Fatty acid synthase (ab22759) and Superoxide dismutase 4 (ab16834) were purchased from Abcam (dilution 1/1000). PPARγ (07-466) was purchased from Millipore (dilution 1/1000).

Supplementary Material

Refer to Web version on PubMed Central for supplementary material.

Acknowledgments

We thank K.C. Hayes and the staff of the Foster Biomedical Research Laboratory at Brandeis University for excellent care of the animals used in this study. We thank the Joslin Diabetes and Endocrinology Research Center Specialized assay (5P30 DK 36836) and Physiology cores, and the Longwood Small Animal Imaging Facility. We also thank Kate Ellacott and the staff of the Vanderbilt Mouse Metabolic Phenotyping Center for the energy expenditure studies. The Vanderbilt MMPC is supported by NIH Grant DK59637. This work was supported by NIH grants (DK31036 and DK82659), DERC grants (DK34834) and an American Diabetes Association mentor-based award.

Reference List

1. Haslam DW, James WP. Obesity. *Lancet*. 2005; 366:1197–1209. [PubMed: 16198769]
2. Cypess AM, et al. Identification and importance of brown adipose tissue in adult humans. *N Engl J Med*. 2009; 360:1509–1517. [PubMed: 19357406]
3. Marken Lichtenbelt WD, et al. Cold-activated brown adipose tissue in healthy men. *N Engl J Med*. 2009; 360:1500–1508. [PubMed: 19357405]
4. Saito M, et al. High incidence of metabolically active brown adipose tissue in healthy adult humans: effects of cold exposure and adiposity. *Diabetes*. 2009; 58:1526–1531. [PubMed: 19401428]
5. Virtanen KA, et al. Functional brown adipose tissue in healthy adults. *N Engl J Med*. 2009; 360:1518–1525. [PubMed: 19357407]
6. Zingaretti MC, et al. The presence of UCP1 demonstrates that metabolically active adipose tissue in the neck of adult humans truly represents brown adipose tissue. *FASEB J*. 2009; 23:3113–3120. [PubMed: 19417078]
7. Poulos SP, Hausman DB, Hausman GJ. The development and endocrine functions of adipose tissue. *Mol Cell Endocrinol*. 2010; 323:20–34. [PubMed: 20025936]
8. Bluher S, Kratzsch J, Kiess W. Insulin-like growth factor I, growth hormone and insulin in white adipose tissue. *Best Pract Res Clin Endocrinol Metab*. 2005; 19:577–587. [PubMed: 16311218]
9. Tseng YH, Kriauciunas KM, Kokkotou E, Kahn CR. Differential roles of insulin receptor substrates in brown adipocyte differentiation. *Mol Cell Biol*. 2004; 24:1918–1929. [PubMed: 14966273]

10. Entingh-Pearsall A, Kahn CR. Differential roles of the insulin and insulin-like growth factor-I (IGF-I) receptors in response to insulin and IGF-I. *J Biol Chem.* 2004; 279:38016–38024. [PubMed: 15247278]
11. Back K, Arnqvist HJ. Changes in insulin and IGF-I receptor expression during differentiation of human preadipocytes. *Growth Horm IGF Res.* 2009; 19:101–111. [PubMed: 18693051]
12. Boucher J, Tseng YH, Kahn CR. Insulin and insulin-like growth factor-1 receptors act as ligand-specific amplitude modulators of a common pathway regulating gene transcription. *J Biol Chem.* 2010; 285:17235–17245. [PubMed: 20360006]
13. Guerra C, et al. Brown adipose tissue-specific insulin receptor knockout shows diabetic phenotype without insulin resistance. *J Clin Invest.* 2001; 108:1205–1213. [PubMed: 11602628]
14. Bluher M, et al. Adipose tissue selective insulin receptor knockout protects against obesity and obesity-related glucose intolerance. *Dev Cell.* 2002; 3:25–38. [PubMed: 12110165]
15. Kloting N, et al. Autocrine IGF-1 action in adipocytes controls systemic IGF-1 concentrations and growth. *Diabetes.* 2008; 57:2074–2082. [PubMed: 18443199]
16. Boucher J. A kinase-independent role for unoccupied insulin and IGF-1 receptors in the control of apoptosis. *Sci Signal.* 2010; 3:ra87. [PubMed: 21139139]
17. Tseng YH, et al. New role of bone morphogenetic protein 7 in brown adipogenesis and energy expenditure. *Nature.* 2008; 454:1000–1004. [PubMed: 18719589]
18. Wu Z, Bucher NLR, Farmer SR. Induction of peroxisome proliferator activated receptor during conversion of 3T3-L1 fibroblasts into adipocytes is mediated by C/EBP β , C/EBP δ , and glucocorticoids. *Mol Cell Biol.* 1996; 16:4128–4136. [PubMed: 8754811]
19. Yeh WC, Cao Z, Classon M, McKnight SL. Cascade regulation of terminal adipocyte differentiation by three members of the C/EBP family of leucine zipper proteins. *Genes Dev.* 1995; 9:168–181. [PubMed: 7531665]
20. Tang QQ, et al. Sequential phosphorylation of CCAAT enhancer-binding protein beta by MAPK and glycogen synthase kinase 3beta is required for adipogenesis. *Proc Natl Acad Sci U S A.* 2005; 102:9766–9771. [PubMed: 15985551]
21. Park BH, Qiang L, Farmer SR. Phosphorylation of C/EBPbeta at a consensus extracellular signal-regulated kinase/glycogen synthase kinase 3 site is required for the induction of adiponectin gene expression during the differentiation of mouse fibroblasts into adipocytes. *Mol Cell Biol.* 2004; 24:8671–8680. [PubMed: 15367685]
22. Tseng YH, Cypess AM, Kahn CR. Cellular bioenergetics as a target for obesity therapy. *Nat Rev Drug Discov.* 2010; 9:465–482. [PubMed: 20514071]
23. Kajimura S, Seale P, Spiegelman BM. Transcriptional control of brown fat development. *Cell Metab.* 2010; 11:257–262. [PubMed: 20374957]
24. Almind K, Manieri M, Sivitz WI, Cinti S, Kahn CR. Ectopic brown adipose tissue in muscle provides a mechanism for differences in risk of metabolic syndrome in mice. *Proc Natl Acad Sci U S A.* 2007; 104:2366–2371. [PubMed: 17283342]
25. Katic M, et al. Mitochondrial gene expression and increased oxidative metabolism: role in increased lifespan of fat-specific insulin receptor knock-out mice. *Aging Cell.* 2007; 6:827–839. [PubMed: 18001293]
26. Petrovic N, et al. Chronic peroxisome proliferator-activated receptor gamma (PPARgamma) activation of epididymally derived white adipocyte cultures reveals a population of thermogenically competent, UCP1-containing adipocytes molecularly distinct from classic brown adipocytes. *J Biol Chem.* 2010; 285:7153–7164. [PubMed: 20028987]
27. Vijgen GH, et al. Brown adipose tissue in morbidly obese subjects. *PLoS ONE.* 2011; 6:e17247. [PubMed: 21390318]
28. Ouellet V, et al. Outdoor temperature, age, sex, body mass index, and diabetic status determine the prevalence, mass, and glucose-uptake activity of ¹⁸F-FDG-detected BAT in humans. *J Clin Endocrinol Metab.* 2011; 96:192–199. [PubMed: 20943785]
29. Pfannenberger C, et al. Impact of age on the relationships of brown adipose tissue with sex and adiposity in humans. *Diabetes.* 2010; 59:1789–1793. [PubMed: 20357363]
30. Enerback S, et al. Mice lacking mitochondrial uncoupling protein are cold-sensitive but not obese. *Nature.* 1997; 387:90–94. [PubMed: 9139827]

31. Liu X, et al. Paradoxical resistance to diet-induced obesity in UCP1-deficient mice. *J Clin Invest.* 2003; 111:399–407. [PubMed: 12569166]
32. Feldmann HM, Golozoubova V, Cannon B, Nedergaard J. UCP1 ablation induces obesity and abolishes diet-induced thermogenesis in mice exempt from thermal stress by living at thermoneutrality. *Cell Metab.* 2009; 9:203–209. [PubMed: 19187776]
33. Golozoubova V, et al. Only UCP1 can mediate adaptive nonshivering thermogenesis in the cold. *FASEB J.* 2001; 15:2048–2050. [PubMed: 11511509]
34. Ukropec J, Anunciado RP, Ravussin Y, Hulver MW, Kozak LP. UCP1-independent thermogenesis in white adipose tissue of cold-acclimated *Ucp1*^{-/-} mice. *J Biol Chem.* 2006; 281:31894–31908. [PubMed: 16914547]
35. Shabalina IG, et al. Cold tolerance of UCP1-ablated mice: a skeletal muscle mitochondria switch toward lipid oxidation with marked UCP3 up-regulation not associated with increased basal, fatty acid- or ROS-induced uncoupling or enhanced GDP effects. *Biochim Biophys Acta.* 2010; 1797:968–980. [PubMed: 20227385]
36. Lowell BB, Spiegelman BM. Towards a molecular understanding of adaptive thermogenesis. *Nature.* 2000; 404:652–660. [PubMed: 10766252]
37. Wijers SL, Saris WH, van Marken Lichtenbelt WD. Recent advances in adaptive thermogenesis: potential implications for the treatment of obesity. *Obes Rev.* 2009; 10:218–226. [PubMed: 19021870]
38. Abel ED, et al. Adipose-selective targeting of the GLUT4 gene impairs insulin action in muscle and liver. *Nature.* 2001; 409:729–733. [PubMed: 11217863]
39. Ueki K, et al. Total insulin and IGF-I resistance in pancreatic beta cells causes overt diabetes. *Nat Genet.* 2006; 38:583–588. [PubMed: 16642022]
40. Norris AW, et al. Muscle-specific PPAR γ -deficient mice develop increased adiposity and insulin resistance but respond to thiazolidinediones. *J Clin Invest.* 2003; 112:608–618. [PubMed: 12925701]

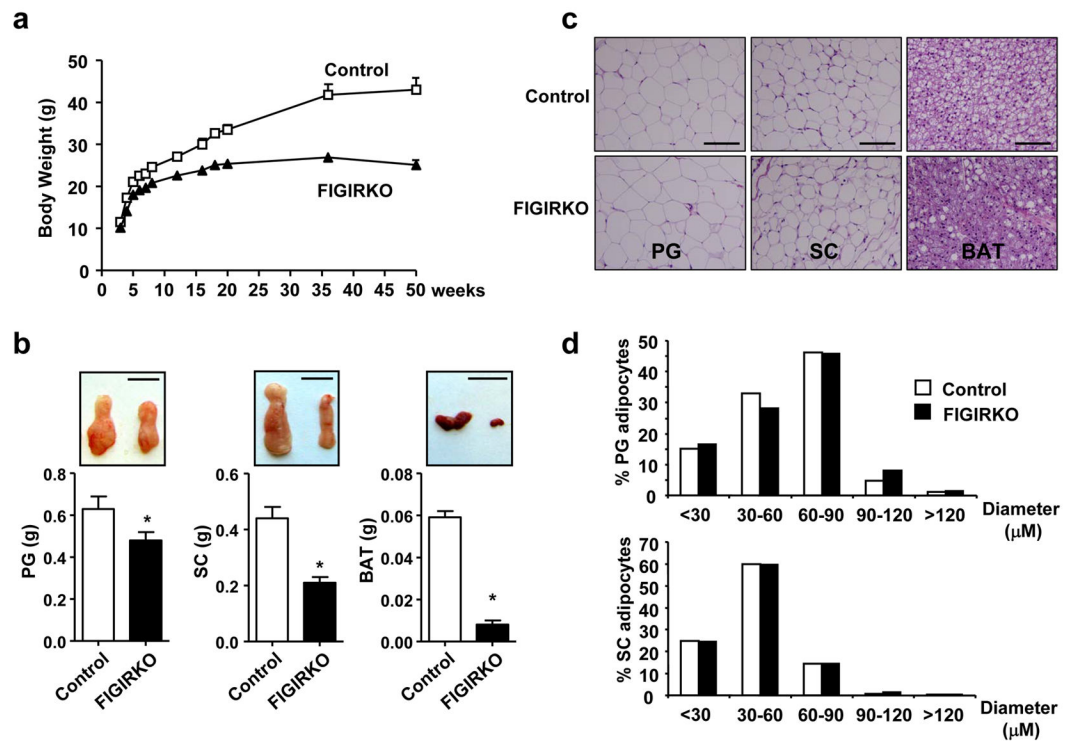


Figure 1. FIGIRKO mice have reduced adiposity

(a) Body weight of male control and FIGIRKO mice fed a chow diet. Results are mean \pm SEM of 8–15 animals/group. (b) Lower panels show perigonadal (PG), inguinal subcutaneous (SC), and brown adipose tissue (BAT) depot weights in 4 months old control and FIGIRKO male mice fed a chow diet. Results are mean \pm SEM of 16–18 animals/group. Upper panels show representative fat pads. Scale bar = 1 cm. (c) Hematoxylin and eosin stained sections of adipose tissues from male control and FIGIRKO at 4 months of age on a chow diet. Scale bar = 100 μm . (d) Diameter distribution of isolated PG and SC adipocytes from 4 months old control and FIGIRKO male mice. Data represent the distribution from \approx 4000 adipocytes from 4 control and 4 FIGIRKO mice. Statistical significance assessed by two-tailed Student's *t* test, * $p < 0.05$.

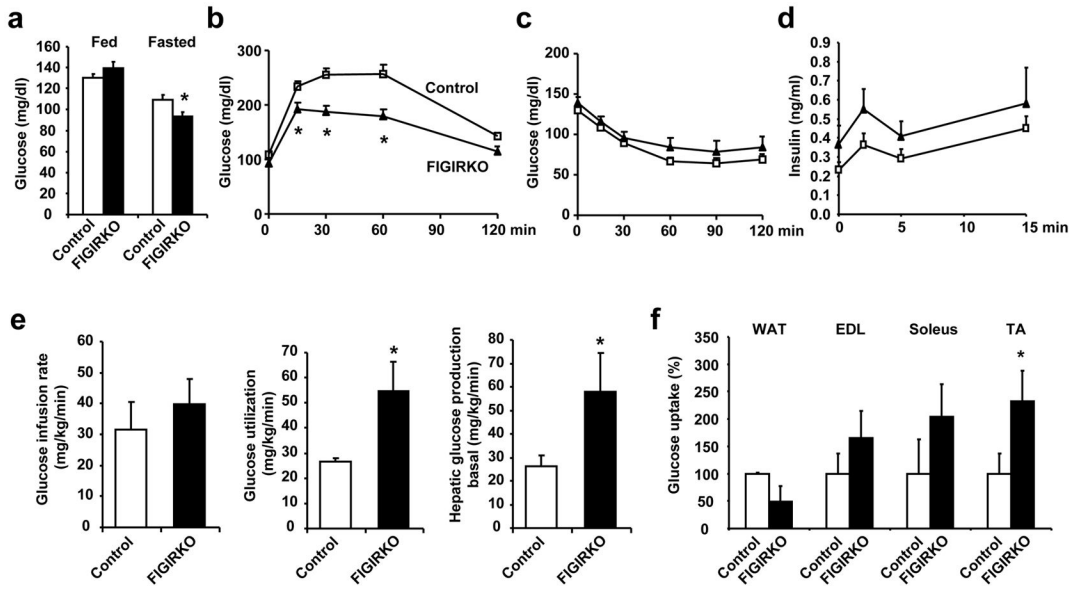


Figure 2. FIGIRKO mice are protected against age-associated glucose intolerance
(a) Fed and fasted blood glucose levels in 1 year old control and FIGIRKO male mice. Results are mean \pm SEM of 7–8 animals/group. **(b)** Intraperitoneal glucose tolerance test and **(c)** Insulin tolerance test performed in 1 year old control and FIGIRKO male mice. Results are mean \pm SEM of 7–8 animals/group. **(d)** First phase insulin secretion in 1 year old male control and FIGIRKO mice. Results are mean \pm SEM of 12 animals/group. **(e)** Glucose infusion rate, glucose utilization, and hepatic glucose production in the basal state, were measured during an hyperinsulinemic-euglycemic clamp. Results are mean \pm SEM of 4 control and 5 FIGIRKO mice. **(f)** Insulin-stimulated ^{14}C -2-deoxyglucose uptake was assessed in perigonadal WAT, extensor digitorum longus (EDL), soleus and tibialis anterior (TA) skeletal muscles, during the final 45 minutes of the hyperinsulinemic-euglycemic clamp. Results are mean \pm SEM of 4 control and 5 FIGIRKO mice. Statistical significance assessed by two-tailed Student's t test, * $p < 0.05$.

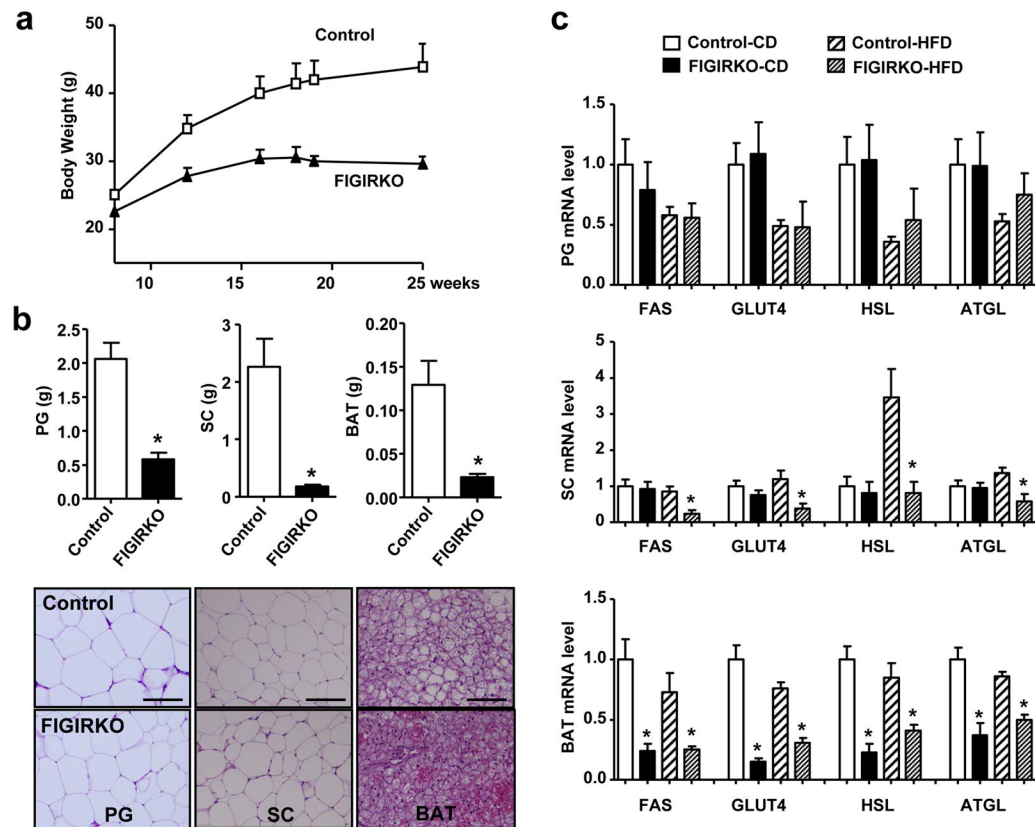


Figure 3. FIGIRKO mice display resistance to high fat diet induced obesity and glucose intolerance

(a) Body weight of control and FIGIRKO mice fed a HFD for 16 weeks. Results are mean \pm SEM of 6 animals/group. (b) Adipose tissue weights (upper panel) and representative hematoxylin and eosin stained sections (lower panel) from perigonadal (PG), inguinal subcutaneous (SC), and brown adipose tissue (BAT) from 6 months old control and FIGIRKO male mice fed a HFD for 4 months. Results are mean \pm SEM of 6 animals/group. Scale bar = 100 μ m (c) *Fas*, *Glut4*, *HSL* and *ATGL* mRNA abundance was measured by real time PCR in perigonadal (PG), subcutaneous (SC), and brown (BAT) adipose tissues in male control and FIGIRKO mice fed either a chow diet (CD) or HFD. Results are mean \pm SEM of 6 animals/group. Statistical significance assessed by two-tailed Student's t test, * $p < 0.05$.

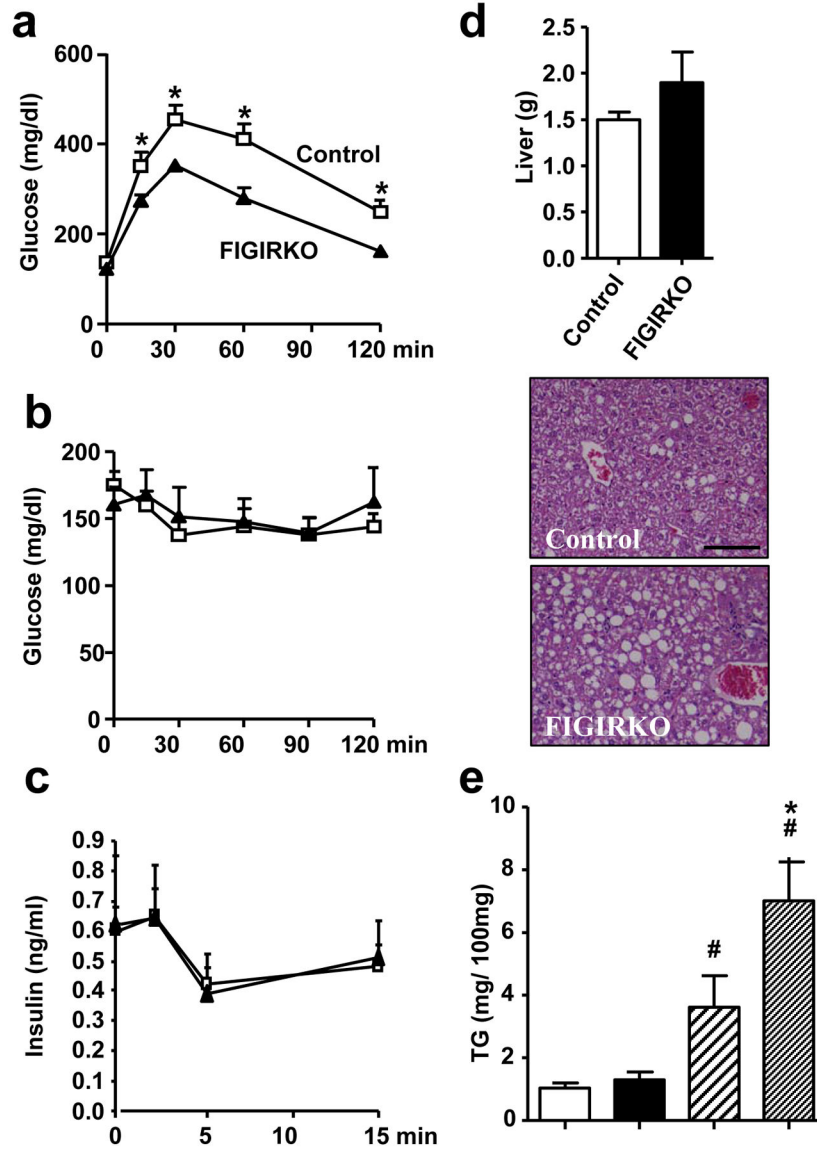


Figure 4. FIGIRKO mice display resistance to high fat diet induced glucose intolerance (a) Intrapерitoneal glucose tolerance, (b) Insulin tolerance and (c) Glucose stimulated insulin secretion tests were performed in 6 months old control and FIGIRKO male mice fed a HFD for 4 months. Results are mean \pm SEM of 6 animals/group. (d) Liver weight (upper panel) and representative hematoxylin and eosin stained section (lower panels) from 6 months old male control and FIGIRKO mice fed a HFD for 4 months. Results are mean \pm SEM of 6 animals/group. Scale bar = 100 μ m. (e) Liver triglyceride content in 6 months old male control and FIGIRKO mice fed either a chow diet (CD) or a HFD. Statistical significance assessed by two-tailed Student's t test, * $p < 0.05$ between control and FIGIRKO mice, # $p < 0.05$ between CD and HFD.

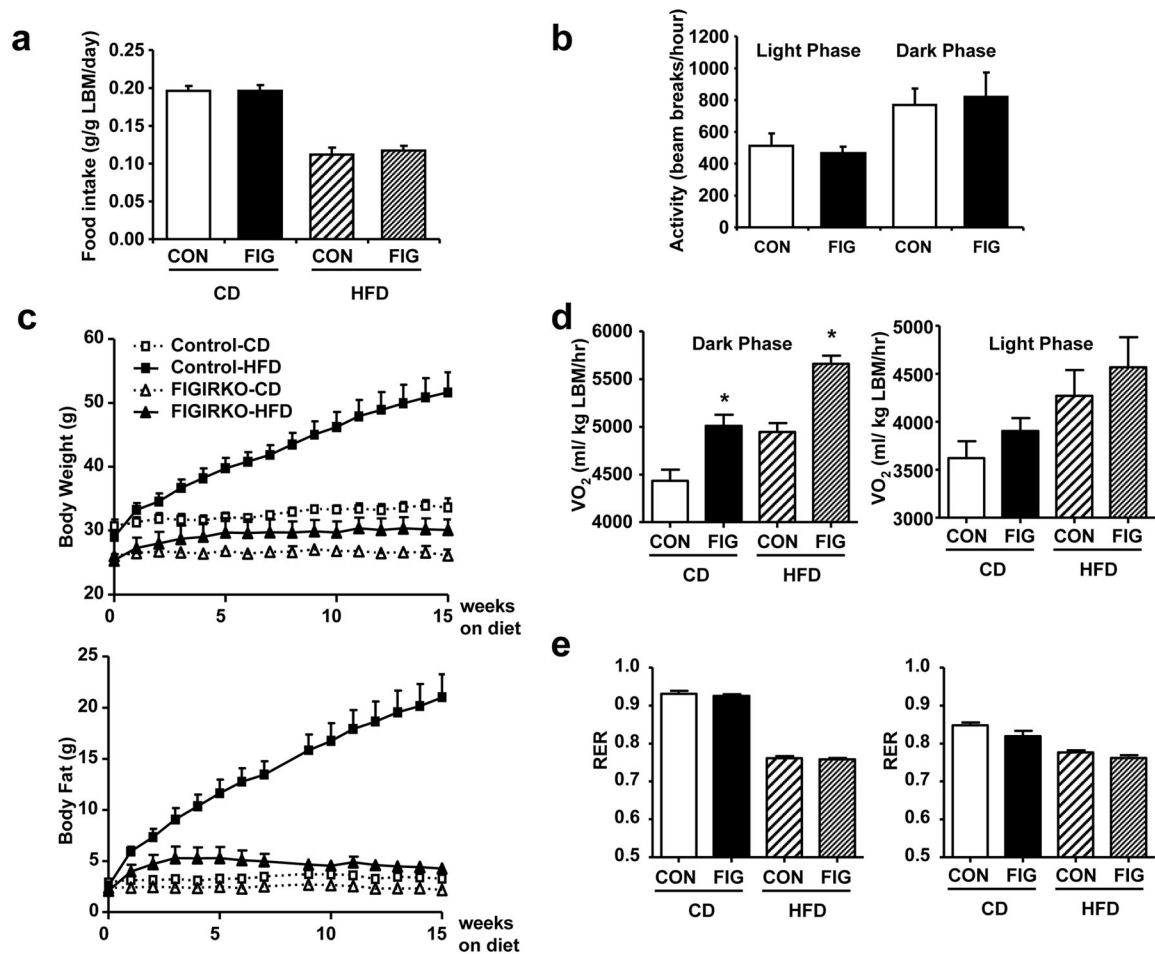


Figure 5. Increased energy expenditure in FIGIRKO mice

(a) Daily food intake was measured in chow diet (CD) or HFD fed control and FIGIRKO male mice. Mice were housed individually and food weight was measured 3 times a week for 2 consecutive weeks. For each mouse daily food intake was averaged and results are mean \pm SEM of 6–8 animals/group. (b) Spontaneous activity was measured in control and FIGIRKO male mice fed a chow diet during 48 hours. Results are mean \pm SEM of 12 animals/group. (c) Body weight and body fat content assessed by nuclear magnetic resonance were measured weekly in 6 months old control and FIGIRKO male mice fed a chow diet or high fat diet for another 4 months. Results are mean \pm SEM of 6 animals/group. (d) Oxygen consumption (VO₂) and (e) respiratory exchange ratio (RER) were analyzed by indirect calorimetry in 10 months old control and FIGIRKO male mice fed a chow diet or a high fat diet for 4 months. Results are mean \pm SEM of 6 animals/group. Statistical significance assessed by two-tailed Student's t test, * $p < 0.05$.

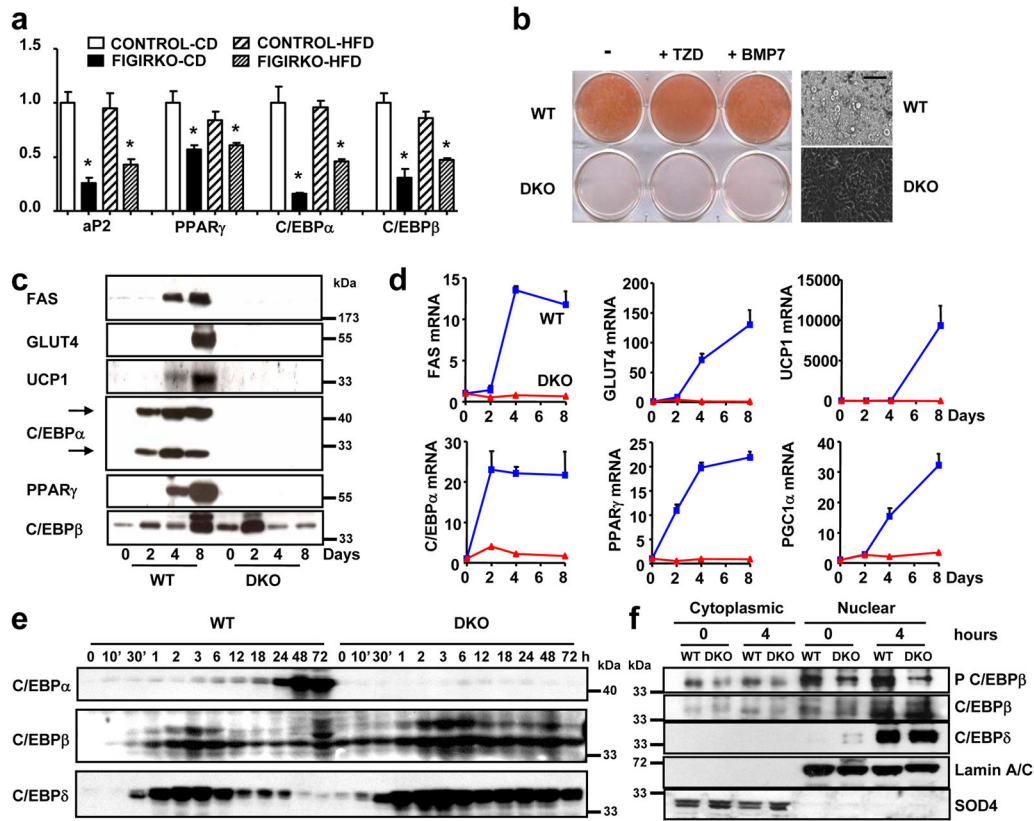


Figure 6. Adipocyte differentiation is impaired in DKO brown preadipocytes
(a) *aP2*, *PPAR γ* , *C/EBP α* and *C/EBP β* mRNA abundance was measured by real time PCR in BAT from control and FIGIRKO male mice fed either a chow or a high fat diet. Results are mean \pm SEM of 6 animals/group. **(b)** Oil Red O staining of WT and DKO brown preadipocyte cells differentiated for 8 days in the presence or in the absence of the thiazolidinedione rosiglitazone (1 μ M) or bone morphogenetic protein 7 (10 nM). A bright field microscopy picture of the differentiated cells is also shown. Scale bar = 100 μ m **(c)** Protein levels measured by western blot in WT and DKO cells before or 2, 4 and 8 days after induction of the differentiation. One representative blot from 3 independent experiments is shown. **(d)** mRNA abundance was measured by real time PCR in WT and DKO cells during the differentiation process before or 2, 4 and 8 days after induction of the differentiation. Results are mean \pm SEM of 4 independent experiments. **(e)** Protein levels measured by western blot in WT and DKO cells during the first 3 days of differentiation. One representative blot from 3 independent experiments is shown. **(f)** Phosphorylation of *C/EBP β* on Thr188, and *C/EBP β* and δ levels were measured in WT and DKO cells in cytoplasmic and nuclear extracts, both in basal conditions and 4 hours after the start of adipogenic conversion. One representative blot from 3 independent experiments is shown. Statistical significance assessed by two-tailed Student's t test, * $p < 0.05$.

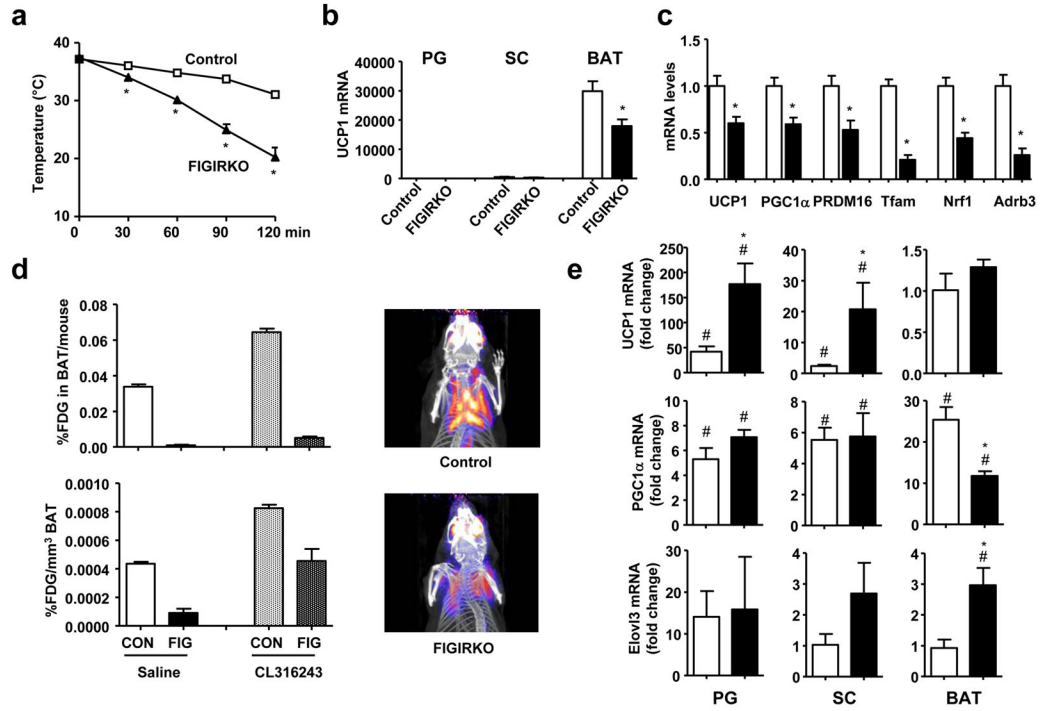


Figure 7. FIGIRKO mice are extremely cold sensitive

(a) Rectal temperature was measured in 4 months old control and FIGIRKO male mice every 30 min for 2 hours after exposure to a 4°C environment (n=9 per group). (b) *UCP1* mRNA abundance was measured by real-time PCR in PG, SC and BAT in 4 months old male control and FIGIRKO mice. (c) mRNA abundance was measured by real-time PCR in BAT from 4 month old control and FIGIRKO male mice. Results are mean ± SEM of 6 animals/group. (d) Control and FIGIRKO mice were anesthetized and injected with 18-FDG. One hour after FDG injection, whole body PET-CT scans were performed and the interscapular area was analyzed to measure FDG uptake in BAT. The experiment was repeated 1 hour after injection of CL316243 (1 µg/g body weight) intraperitoneally. Results are mean ± SEM of 2 animals/group. Right panel show three-dimensional reconstruction images of control and FIGIRKO mice after FDG injection in the basal state. (e) *UCP1*, *PGC1α* and *Elov3* mRNA abundance was measured by real time PCR in PG, SC and BAT in 4 months old control and FIGIRKO male mice injected with either saline or CL316243 (1 µg/g body weight) intraperitoneally. Results are mean ± SEM of 5 animals/group and are expressed as fold change over the saline group. Statistical significance assessed by two-tailed Student’s t test, * p<0.05 between control and FIGIRKO mice, # p<0.05 between saline and CL316243 treated group.

Table 1
Serum parameters in chow diet or HFD fed control and FIGIRKO mice

Circulating concentrations were measured in control and FIGIRKO male mice fed a regular chow diet or HFD for 4 months (6–10 animals per group) in the fed state.

	Chow diet		High fat diet	
	Control	FIGIRKO	Control	FIGIRKO
Insulin (ng/ml)	0.86 ± 0.10	0.98 ± 0.13	1.40 ± 0.58	8.42 ± 3.25*
IGF-1 (ng/ml)	560 ± 32	475 ± 24	387 ± 47	402 ± 29
TG (mg/dl)	67 ± 11	88 ± 12	89 ± 6	144 ± 27
FFA (mEq/ml)	1.92 ± 0.19	2.36 ± 0.17	1.54 ± 0.25	2.70 ± 0.58
Cholesterol (mg/dl)	109 ± 5	109 ± 7	169 ± 11	157 ± 21
Leptin (ng/ml)	4.7 ± 0.8	2.7 ± 0.4*	20.8 ± 6.1	8.4 ± 1.8*
Resistin (ng/ml)	1.28 ± 0.12	1.22 ± 0.07	0.74 ± 0.08	0.33 ± 0.08*
Adiponectin (µg/ml)	22.3 ± 2.5	18.4 ± 3.0	17.9 ± 1.2	10.5 ± 1.4*
TNFα (pg/ml)	3.9 ± 0.3	4.4 ± 0.3	4.2 ± 0.3	4.8 ± 0.6
PAI-1 (ng/ml)	0.95 ± 0.14	0.82 ± 0.13	1.49 ± 0.10	1.44 ± 0.48
IL6 (pg/ml)	7.6 ± 0.5	9.7 ± 2.1	9.0 ± 1.8	9.3 ± 2.2

Results are mean ± SEM. Statistical significance assessed by two-tailed Student's t test.

* p<0.05 between control and FIGIRKO mice.